IET Nanobiotechnology

Research Article

IET Journals
The Institution of Engineering and Technology

Folate encapsulation in PEG-diamine grafted mesoporous Fe_3O_4 nanoparticles for hyperthermia and in vitro assessment

ISSN 1751-8741
Received on 17th March 2020
Revised 28th July 2020
Accepted on 2nd October 2020
E-First on 4th November 2020
doi: 10.1049/iet-nbt.2020.0101
www.ietdl.org

Ahmaduddin Khan[1], Niroj Kumar Sahu[1] ✉

[1]*Centre for Nanotechnology Research, Vellore Institute of Technology, Vellore 632014, TN, India*

✉ *E-mail: nirojs@vit.ac.in*

Abstract: Effective and targeted delivery of the antitumour drugs towards the specific cancer spot is the major motive of drug delivery. In this direction, suitably functionalised magnetic iron oxide nanoparticles (NPs) have been utilised as a theranostic agent for imaging, hyperthermia and drug delivery applications. Herein, the authors reported the preparation of multifunctional polyethyleneglycol-diamine functionalised mesoporous superparamagnetic iron oxide NPs (SPION) prepared by a facile solvothermal method for biomedical applications. To endow targeting ability towards tumour site, folic acid (FA) is attached to the amine groups which are present on the NPs surface by 1-ethyl-3-(3-dimethylaminopropyl) carbodiimide hydrochloride/N-hydroxysuccinimide chemistry. FA attached SPION shows good colloidal stability and possesses high drug-loading efficiency of ~ 96% owing to its mesoporous nature and the electrostatic attachment of daunosamine (NH_3^+) group of doxorubicin (DOX) towards the negative surface charge of carboxyl and hydroxyl group. The NPs possess superior magnetic properties in result endowed with high hyperthermic ability under alternating magnetic field reaching the hyperthermic temperature of 43°C within 223 s at NP's concentration of 1 mg/ml. The functionalised NPs possess non-appreciable toxicity in breast cancer cells (MCF-7) which is triggered under DOX-loaded SPION.

1 Introduction

Chemotherapy is a traditional treatment process, which causes an adverse toxic effect on the whole body and also has a low therapeutic effect. Nanoparticles (NPs) which are functionalised with surface moiety and loaded with the antitumour drug have been used to increase the therapeutic efficacy along with lesser side effect [1–4]. Superparamagnetic iron oxide NPs (SPION) are extensively used as antitumour drug cargo and magnetic resonance imaging (MRI) contrast agent for the development of therapeutic platforms, imaging and diagnosis simultaneously [4–8]. Different kind of nanostructures like carbon nanotube [9], gold nanoshells [10], magnetic NPs [11], graphene [12] etc. have been explored vastly as chemotherapeutic drug cargo for tumour therapy [13]. Among them, magnetic NPs have been used extensively because of its magnetic manipulation, MRI signal, better biocompatibility, ability to generate heat because of the alternating current magnetic field (ACMF) and degradation in acidic conditions [4, 13–16]. Proper functionalisation of NPs is the main factor to ensure colloidal stability and their utilisation in biomedical applications [16–19]. Various biocompatible polymers such as poly(N-isopropyl-acrylamide) [20, 21], alginate [22], dextran [23] etc. are used to modify the surface of magnetic NPs to increase the efficacy of the carrier. Moreover, to carry a substantial quantity of drug towards specific tumour location and to decrease the toxicity of anticancer drug, hollow and mesoporous NPs are utilised since they exhibit high porosity, more specific surface area and enormous active sites [16, 24, 25]. Magnetic NPs conjugated with some targeting moieties manifest great ability for specific drug delivery. Targeting ligands endow the NPs for specific binding of anti-cancerous drug carrier to the surface of the cell through receptor-mediated endocytosis thereby enhancing cellular uptake [26, 27].

Folic acid (FA) having lesser molecular weight is a stable, non-toxic and inexpensive non-immunogenic receptor-specific ligand for the antitumour therapeutics as many human cancer cells overexpress on folate receptors unlike normal cells [26, 28, 29]. Huang *et al.* [4] reported FA-anchored SPIONs loaded with doxorubicin (DOX) and tested on MCF-7 breast cancer cells. The maximum inhibition efficiency of DOX@FA-SPION was observed in presence of the magnetic field. Gupta *et al.* [26] reported polyacrylic acid functionalised Fe_3O_4 NPs attached with FA by peptide bond between carboxyl group present on the NPs surface and amine group of FA. Results obtained from the confocal microscopy and flow cytometry showed that there was ~61.3% of HeLa cells apoptosis when treated with drug-loaded Fe_3O_4 NPs because of the disintegration of DNA. They further showed that the introduction of magnetic hyperthermia results in an increase cells apoptosis to ~95% [26]. In a report, iron oxide condensed colloidal magnetic nanocluster functionalised with FA was studied for specific DOX delivery on the cancerous cells which shows the overexpression of folate receptor [30]. Condensed magnetic NPs were coated with alginate and polyethylene glycol (PEG) was conjugated onto the carboxyl end group of alginates. Terminal OH group of PEG was utilised for folate conjugation. The DOX-loaded FA attached NPs show enhanced uptake and maximum cytotoxicity on MDA-MB-231 cells having folate overexpression as compared to MCF-7 which does not express folate receptor [30]. Yang *et al.* [31] reported FA-grafted chitosan-coated magnetic NPs loaded with DOX that possessed significant toxicity than without FA coating or when only DOX was used [31].

The FA receptor-based mechanism forms a certain target which is useful for particular tumour targeted drug delivery since many cancers show its upregulation which includes the ovary, breast, lung, kidney and brain. As the grade/stage of cancer increases, the density of FA receptor also appears to increase [32, 33]. A secondary feature of FA receptor which is useful for intravenous drug delivery is only after malignant transformation the FA receptor gets approachable to the vascular epithelium. The reason behind this is the surface of the apical membrane of normal polarised epithelial cells shows a particular expression of FA receptor, thus it is safe from FA receptor directed drugs which are delivered in the plasma. However, after the transformation of epithelial cells, the polarity of the cell is lost and FA receptor gets accessible to the targeted drugs [33, 34].

In the present work, targeting strategy of NPs attached with FA has been reported which provides both specificity and better internalisation of NPs into the cancerous cells. Herein, we report a highly aqueous dispersible, biocompatible mesoporous SPION

synthesised by a simple solvothermal method where PEG-diamine was used as a stabilising agent. Further DOX is loaded on FA functionalised SPION (FA-SPION) and in vitro cytotoxicity has been assessed on MCF-7 cells. The magneto thermal induction of the SPION has been evaluated for possible combined therapy.

2 Experimental section

2.1 Reagents and materials

All the chemicals are used as received. Iron chloride hexahydrate ($FeCl_3.6H_2O$), iron chloride tetrahydrate ($FeCl_2.4H_2O$), PEG diamine (NH_2–PEG–NH_2), hydrazine hydrate (NH_2–NH_2), 1-ethyl-3-(3-dimethylaminopropyl) carbodiimide hydrochloride (EDC), folic acid (FA) and dimethyl sulfoxide (DMSO) are procured from Sigma Aldrich, India. Dulbecco modified eagle medium (DMEM), N-hydroxysuccinimide (NHS), penicillin streptomycin solution, 3-(4,5-dimethylthiazol-2-yl)-2,5-diphenyltetrazolium bromide (MTT) are obtained from HiMedia, India. Ethylene glycol (EG) is obtained from Sisco research laboratories (SRL), India. Sodium hydroxide (NaOH) is obtained from SDfine chemicals, India and DOX is obtained from Alfa Aesar, India. MCF-7 (human breast cancer) cell line is acquired from NCCS Pune, India. Distilled water is utilised throughout the experiment.

2.2 Preparation of mesoporous SPION

The SPION is prepared by using a solvothermal method. At first, 730 mg of $FeCl_3.6H_2O$ and 270 mg of $FeCl_2.4H_2O$ is added to 50 ml of EG to form homogeneous solution. Then 10 ml of PEG-diamine (50 mg/10 ml of EG) is added as a capping agent. After that, the above mixture is vigorously stirred for 60 min at 1000 rpm in an inert condition. Then, 5 ml of hydrazine hydrate is added to form a black homogeneous solution. Further, it is transferred to a Teflon container and sealed in an airtight autoclave and heated for 200 °C for 12 h. Then it is cooled down to room temperature and the precipitates are collected by magnetic separation method. Finally, the material is dried overnight at room temperature.

2.3 Preparation of FA-SPION

Attachment of FA to SPION is carried out through the reported procedure with slight modification [35]. To anchor FA onto the surface of SPION, 70.6 mg of FA is dissolved in 10 ml of distilled water–DMSO solution (1:1 v/v) and its pH is adjusted to 8 by diluted NaOH. Further, 65.92 mg of EDC and 36.83 mg of NHS is added to the above solution and the pH was maintained in the range of 7.0–8.0. It was stirred continuously for 8–12 h in dark conditions. After that, SPION (50 mg/5 ml) is dispersed in water and added slowly to the FA solution and slowly shaken for 24 h in the dark environment. Finally, FA-SPION is separated magnetically and washed with distilled water multiple times to separate the free FA and further, the sample is dried overnight at room temperature.

2.4 Preparation of DOX@FA-SPION

To load DOX, 10 mg of FA-SPION is dispersed in 2 ml of distilled water and sonicated. After that 50 µl of DOX (concentration, 1 mg/ml) is added and total volume is made up to 3 ml. It is gently shaken overnight in dark condition for 24 h. DOX-loaded FA-SPION is magnetically separated and the fluorescent spectra of supernatant was recorded in order to calculate the entrapment efficiency (EE). The quantity of DOX in the supernatant is calculated by using fluorescence (FL) emission at 562 nm. Furthermore, the percentage of EE was calculated by using the following formula

$$\text{EE}\ \% = \frac{\text{Weight of loaded DOX}}{\text{Weight of total DOX}} \times 100 \tag{1}$$

2.5 Characterisation techniques

X-ray diffraction (XRD) (D8 Advanced, Bruker) with CuK_α radiation is used to study the structure, phase and purity of the formed Fe_3O_4 NPs. Debye Scherer equation is used for the calculation of crystallite size. Fourier transform infrared (FTIR) (IR Affinity-1, Shimadzu) spectra are scanned in the range of 400–4000 cm^{-1}. Thermogravimetric analysis (TGA) (SDT Q600, TA instrument) is used for the thermal analysis of the prepared samples. Field emission scanning electron microscopy (FESEM) (SIGMA HV-Carl Zeiss) is used to study the shape and size of the formed NPs. Energy dispersive X-ray analysis (EDX) (Bruker Quantax 200-Z10) is used to confirm the composition of the material. Vibration sample magnetometer (VSM) (Lake Shore Cryotronics) is used to study magnetisation of the samples. Brunauer Emmett Teller (BET) and Barrett Joyner Halenda (BJH) techniques (Quantachrome Nova Station 1000 instrument) are used to study the pore size, pore volume distribution and specific surface area. Zeta potential of the NPs is determined by litesizer-500 Anton paar, Hyperthermia study is done by Ambrell EASYHEAT 8310 by keeping current and frequency constant. Hitachi F-7000 FL spectrophotometer is used to record FL spectra for evaluating the DOX loading.

2.6 In vitro cytotoxicity studies and cell culture

In vitro cytotoxicity studies are done on MCF-7 breast cancer cells. Cells are harvested in a 96 well plate having a concentration of 1×10^4 cells/well in DMEM with 1X antibiotic antimycotic solution and 10% FBS and kept at 37 °C in CO_2 incubator with 5% CO_2. The cells are further washed with 200 µl 1X PBS and treated with different concentrations of the material in serum-free media with an incubation period of 24 h. The medium was later aspirated from the cells after 24 h. MTT (concentration 0.5 mg/ml in 1X PBS) is added and incubated again for 4 h at 37 °C. Medium containing MTT is discarded and again the cells are washed with 200 µl PBS. To dissolve the formazan crystals 100 µl DMSO is added and mixed thoroughly. The colour intensity developed is assessed at the absorbance of 570 nm by a microplate reader. All experiments are done in triplicate. The viable cells percentage is calculated using the following equation

$$\text{Cell viability}\ \% = \frac{\text{Absorbance of treated cells}}{\text{Absorbance of control cells}} \times 100 \tag{2}$$

2.7 Heating ability of SPION by specific absorption rate (SAR)

The heating potential of SPION is studied by the SAR method depends on time by exposing the different concentrations of material to ACMF (frequency = 312 kHz and current = 235.2 amps). In total, 0.5 and 1 mg/ml concentrations of material are prepared and sonicated thoroughly. Further, the samples are exposed under ACMF until the material reaches the hyperthermic temperature (∼ 43°C). The SAR value is calculated by the following equation

$$\text{SAR} = C_{\text{water}} \times \frac{\Delta \text{T}}{\Delta t} \times \frac{1}{m} \tag{3}$$

where C_{water}, $\Delta T/\Delta t$ and m are the specific heat capacity, the initial slope of the time-dependent temperature curve and mass of the prepared NPs, respectively.

3 Results and discussion

3.1 Physical characterisation

Fig. 1*a* shows the XRD pattern of SPION, matches with JCPDS card no: 19–0629, which indicates the inverse spinel structure formation. The absence of any extra peaks in the XRD pattern conveys the sample purity. Crystallite size of SPION is calculated by Debye Scherrer formula from the most prominent peak (311) and is found to be around 19.88 nm. Presence of high intensity

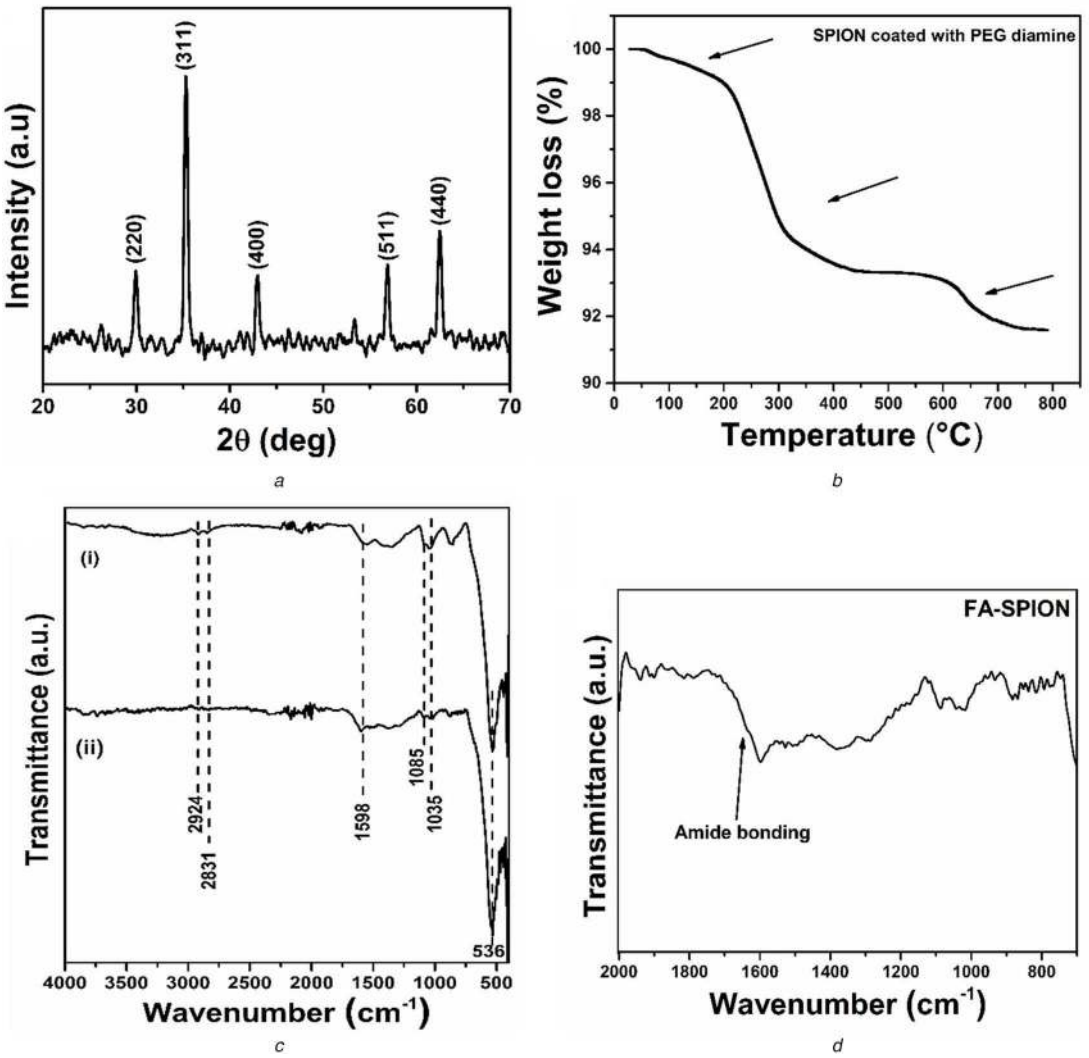

Fig. 1 *Characterisation of prepared NPs*
(a) XRD plot,
(b) TGA plot of SPION,
(c) FTIR spectra of (i) SPION and (ii) FA-SPION,
(d) Enlargement of FA-SPION

peaks suggest the crystalline nature of the prepared NPs. The polymer coating, functionalisation and material's stability are studied by TGA analysis. Fig. 1*b* shows the sequential weight loss of the material with the temperature. Weight loss at a lower temperature (<100°C) is about 0.3% may be due to the removal of physically adsorbed water from the surface. There is a maximum weight loss of nearly 6.12% observed till 400 °C which can be attributed to thermal decomposition of organic compounds [36]. Furthermore, a slight weight loss is detected after 600°C which may be due to the phase transition or buoyancy factor. This phase transition is mainly observed from 600 to 800°C ascribed to the transformation of Fe_3O_4 to FeO (α-Fe_2O_3 and γ-Fe_2O_3) [37].

Fig. 1*c*(i, ii) shows the FTIR spectra of SPION and FA-SPION. Presence of vibrational bands at 1085 and 1035 cm^{-1} show C–N stretch as well as C–O stretch vibration which can be due to coating of PEG-diamine and EG respectively. A sharp peak at 1598 cm^{-1} shows the presence of aromatic ring [26]. A small bend at 1635 cm^{-1} (Fig. 1*d*) indicates amide bond formation between the amine group of PEG-diamine and the carboxyl group of FA [38]. The bands at 2831 and 2924 cm^{-1} in Fig. 1*c*(i) suggest the presence of symmetric and asymmetric CH_2 vibration of the PEG group. Presence of broadband around 3010–3500 cm^{-1} indicates stretching vibration of OH group and NH_2 group [38, 39]. Further, the vibrational band at 532 cm^{-1} correspond to Fe-O vibration indicating the formation of magnetite phase [39].

The FA conjugation was done by EDC/NHS method. EDC reacts with the carboxyl group of FA and forms active o-acylisourea intermediate. It displaces the primary amine present on the NPs surface and forms the amide bond. NHS is further used along with EDC to improve the efficiency of coupling, since, o-acylisourea intermediate is unstable in aqueous solutions. The addition of NHS leads to the formation of NHS ester with the carboxyl group of FA which is more stable than o-acylisourea intermediate thus allowing the formation of stable amide bond [40].

Figs. 2*a* and *b* demonstrate the FESEM images of SPION at different magnification which reveals that the particles are of spherical shape and having size around 102 nm. Size of the NPs is <200 nm which is preferable for drug delivery application and also ensure the use of SPION as nanocarrier [41, 42]. Furthermore, the spherical shape of the NPs increases cellular uptake due to its smaller contact area with respect to the cell membrane receptors [43]. This results in the availability of more number of receptor sites for binding [43, 44]. Presence of only Fe and O in the elemental composition of SPION indicates the purity of the material (Fig. 2*c*). The wt% of 71.08 and 28.92% are found corresponds to iron and oxygen in the EDX data of synthesised particles. Moreover, the atomic % of Fe (41.32%) and O (58.68%) further confirms the formation of Fe_3O_4 NPs with proper stoichiometry [45].

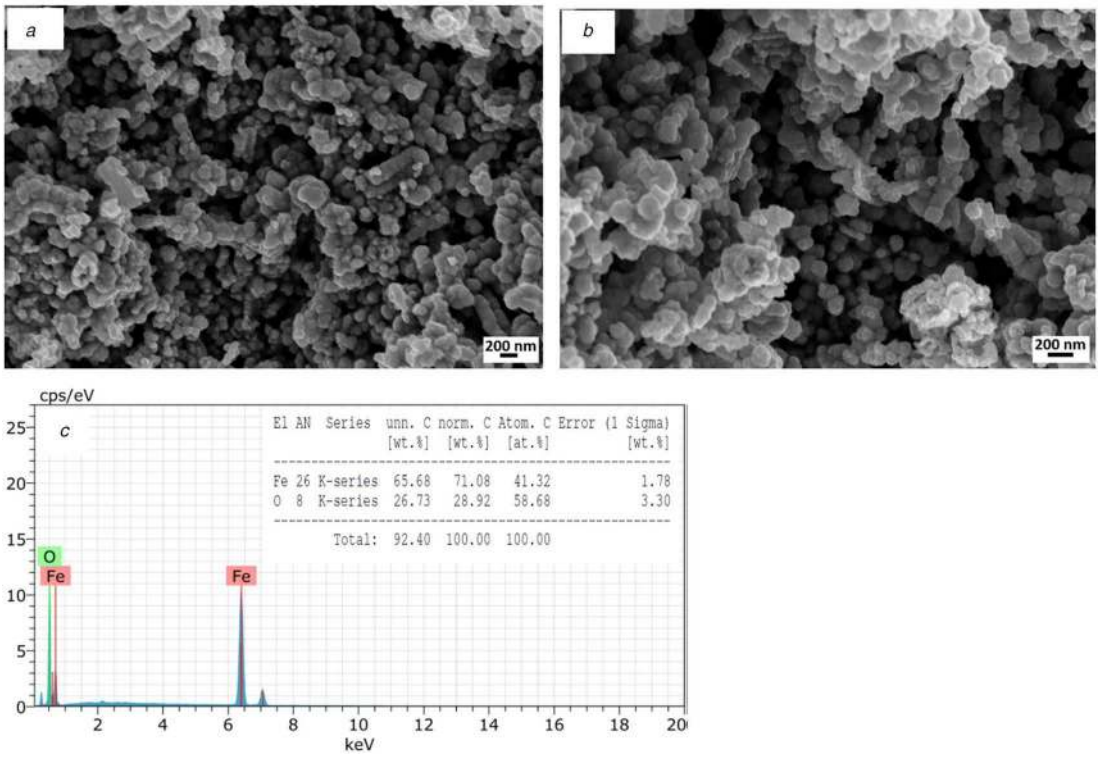

Fig. 2 *FESEM images of SPION at magnification*
(a) 50.00 KX,
(b) 75.00 KX,
(c) EDX spectra

The N_2 adsorption–desorption isotherm is plotted and shown in Fig. 3*a*. The isotherm of SPION resembles to type IV according to IUPAC classification with H3 hysteresis where the relative pressure (P/P_0) is in the range of 0.5–1.0. This indicates the monolayer- multilayer adsorption of the material since it follows the same path at low pressure [46]. The BET surface area and average pore size are found to be 17.4 m^2/g and 3.6 nm, respectively. Pore diameter lies in the range of 2–50 nm confirms the formation of mesoporous NPs. The mesoporous nature with particle size <200 nm makes it a perfect candidate for antitumour drug delivery application.

The surface charges of prepared particles are analysed by zeta potential techniques. Since the Fe_3O_4 NPs is prepared in glycol medium have inherent negative surface due to the presence of OH^- groups. However, zeta potential of SPION is positive and the value is equal to 5.8 mV which confirms the successive coating of amine groups over the SPION. Zeta potential of FA-SPION was found to be negative which indicates the presence of carboxyl group over the FA-SPION [35, 41, 47]. The attachment of FA was further confirmed by UV absorbance spectra (Fig. 3*b*). The occurrence of FA characteristic absorption peaks at 280 and 370 nm in FA-SPION with some shift indicates the successful attachment of FA to SPION [26]. Further, the effect of FA conjugation on SPION was examined by calculating the saturation magnetisation of the SPION and FA-SPION (Fig. 3*c*). Both the NPs show superparamagnetic characteristics possessing high saturation magnetisation of ∼78 and 76 emu/g, respectively. There is a slight decrement in magnetisation value observed in the case of FA-SPION which signifies the anchoring of FA [26]. Magnetic moment value of SPION and FA-SPION is estimated to be 3.24 and 3.14 μ_B/NPs, respectively. The magnetic susceptibility for SPION and FA-SPION at room temperature is 0.094 and 0.091 emu/g Oe, respectively.

3.2 Evaluation of the heating ability of SPION in ACMF

Fig. 4 shows the time-dependent heating ability of SPION with the application of ACMF of frequency 312 kHz and current 235.2 A. Different concentration of SPION (0.5 and 1 mg/ml) have been taken for analysing the heating ability of material which is generated by applying the magnetic field. SPION shows the substantial rate of increase in temperature to reach >40°C which is a necessary condition for therapeutic hyperthermia. SPION having 1 mg/ml concentration is exhibiting effective hyperthermia response than the lower concentration. Since it is attaining the desired temperature within 223 s, whereas the lower concentration of SPION took ∼635 s to reach hyperthermic temperature. The SAR values of SPION at concentrations 0.5 and 1 mg/ml were found to be 137.3 and 208.46 W/g^{-1}, respectively. The higher values of SAR are probably because of surface functionalisation which results in better dispersibility of magnetic particles in the aqueous medium with high colloidal stability [48]. Hyperthermia testing is more advantageous when it is used along with chemotherapy since it breaks the bond (thermoresponsive) between drug and particles with the exposure of ACMF. This results in more drug release. ACMF can cause disruption in the cytoplasmic regions due to noteworthy quantity of drug accumulation in the nucleus. It can also damage various cellular components such as the cytoskeleton, cell membrane and the enzymes used for the synthesis of DNA [26, 48, 49].

3.3 In vitro drug loading and cell culture studies

DOX, a cationic drug is utilised as a model drug for loading into the NPs and anticancer studies. The drug gets loaded because of the electrostatic interaction between the positive daunosamine group of DOX and negative OH^- group from EG in neutral pH [48]. There is a possibility of the hydrogen bond between polar groups of DOX and free NH_2 and OH groups present on the surface of FA-SPION [50, 51]. After magnetic separation, the supernatant was used to measure the EE % of DOX onto the SPION. SPION shows high drug loading efficiency of 96.18% ± 0.246. Appreciable quantity of DOX got loaded mainly due to its mesoporous nature and high specific surface area. The cytotoxicity of SPION was studied on MCF-7 cancer cells (Fig. 5*a*). No appreciable cytotoxicity has been noticed up to a concentration of 500 µg/ml, however there is a modest decrement in the viability at a concentration of 1000 µg/ml. 15.23% inhibition is there probably

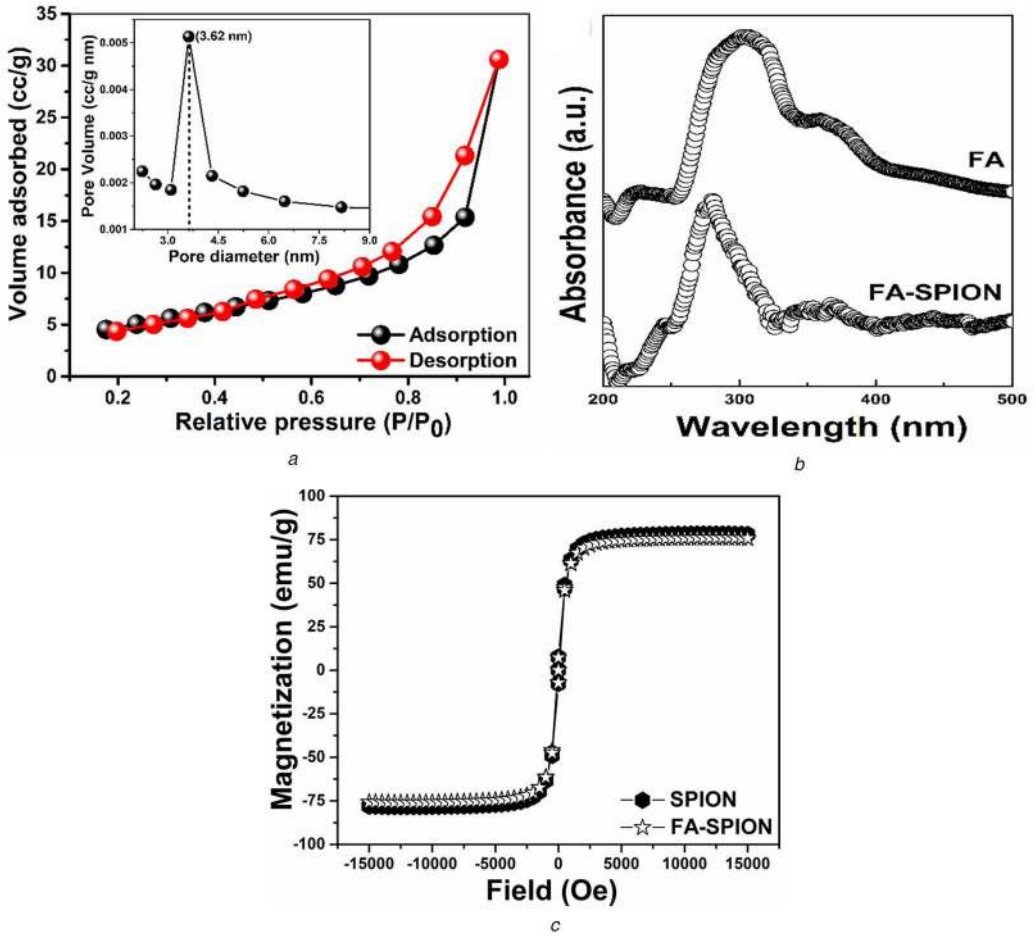

Fig. 3 *Physical characterisation of synthesised NPs*
(a) N_2 adsorption–desorption isotherm with pore size distribution (inset) of SPION,
(b) UV–vis spectra of FA and FA-SPION,
(c) *M–H* loops for SPION and FA-SPION at room temperature

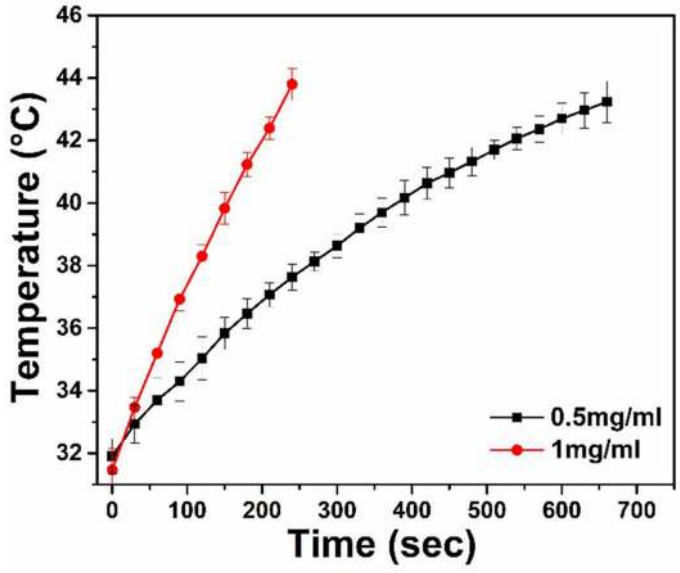

Fig. 4 *Temperature versus time graph of SPION with different concentration at frequency of 312 kHz and current of 235.2 A*

because of the formation of reactive oxygen species (ROS). Peroxide decomposition catalysed by Fe is called a Fenton reaction and is responsible for the formation of ROS like hydroxyl radical (·OH). Such ROS can oxidise several organic moieties such as DNA, proteins and membrane lipids [52–54]. Optical images of MCF-7 cells treated with SPION (Fig. 5*b*) does not show any changes in morphology. In cytotoxicity analysis, (Fig. 6*a*) of MCF-7 cells, shows a decrease in viability when treated with DOX@FA-SPION with different concentration due to release of DOX in the cells. There is a 55.62% inhibition rate when treated with the maximum concentration of 1000 µg/ml. There is a catastrophic cell death upon treatment with DOX@FA-SPION due to sustained release of DOX. The respective DOX concentrations for the DOX@FA-SPION at 1000, 750, 500, 250 and 100 µg/ml are 4.79, 3.59, 2.39, 1.19 and 0.47 µg/ml. DOX decrease the expression of antiapoptotic BCl_2 protein and affects the oxidative

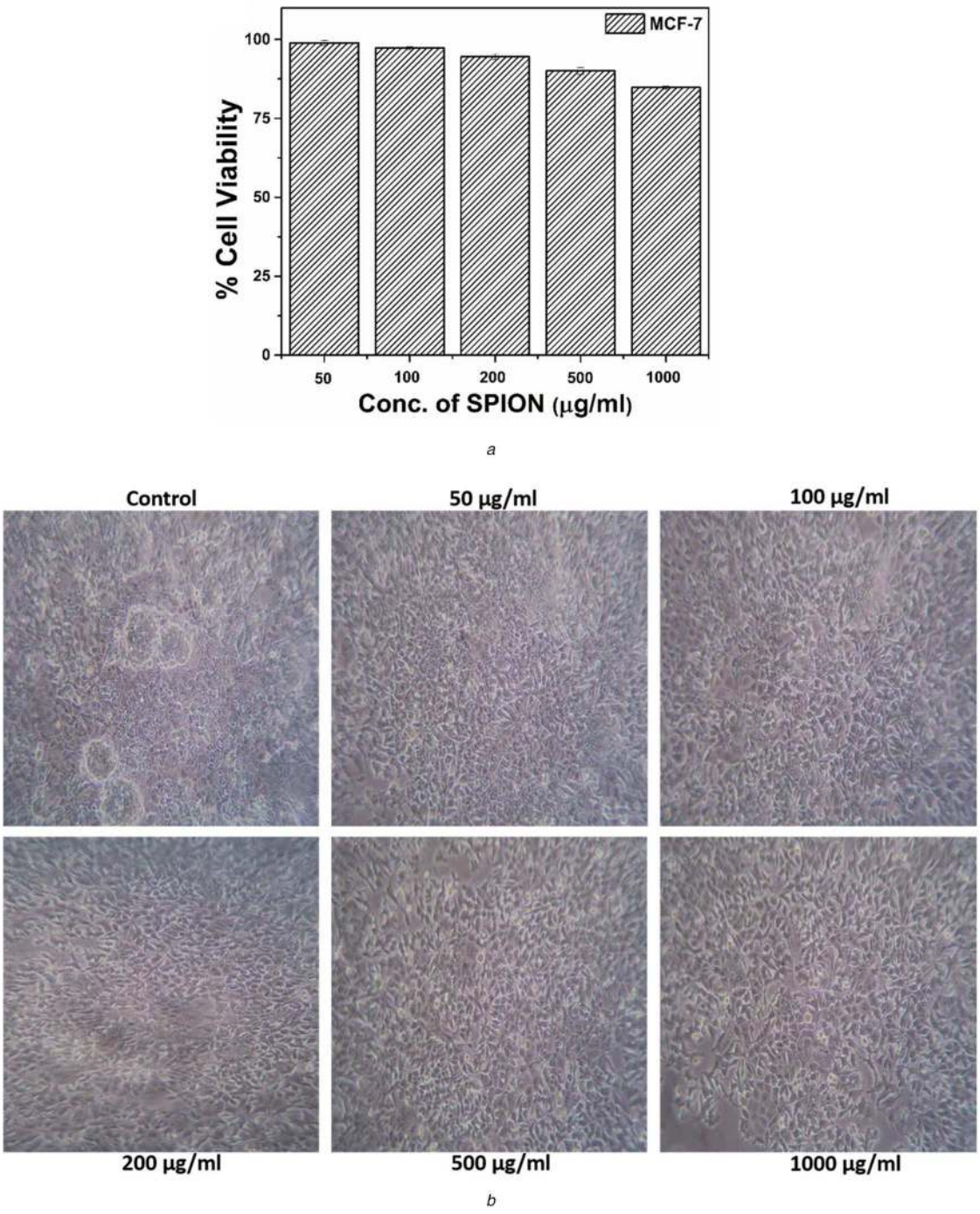

Fig. 5 *Viability after 24 h*
(a) In vitro cytotoxicity,
(b) Optical images of SPION with different concentration against MCF-7 breast cancer cells

stress by enhancing the production of hydrogen peroxide and decreasing NF-kB gene and expression of protein [55]. Higher apoptosis is mainly because of enhanced cellular uptake of drug-loaded NPs due to the active targeting because of FA. DOX@FA-SPION can enter the cells through receptor-mediated endocytosis while bare NPs or free DOX can enter only passively [4]. Optical images (Fig. 6*b*) shows slight changes in morphology as the cells are becoming little shrink and clear patches are visible which corresponds to the cellular apoptosis.

4 Conclusion

Mesoporous particles with high-magnetic saturation are solvothermally prepared and tested for DOX delivery and hyperthermia applications. Prepared particles are having a spherical shape with the size of ∼102 nm. The particles exhibit high DOX-loading efficiency due to its size, mesoporous nature and surface area. It also displays high heating ability towards reaching hyperthermic temperature within 223 s at a concentration of 1 mg/ml. FTIR, UV, zeta potential and VSM data confirm the conjugation of FA to SPION. Attachment of FA increases the drug accumulation in the tumorous cells in comparison to the normal cells because of active targeting ability of FA. The material further shows high cellular apoptosis towards MCF-7 breast cancer cells. This formulation can be more useful when used for both drug delivery and hyperthermia since the chemothermal therapy increases the efficiency by the synergistic effect.

5 Acknowledgment

The authors gratefully acknowledge the financial support from the Indian Council of Medical Research (ICMR) (45/69/2019-Nan/BMS), the DST-SERB (Project No. ECR/2016/000301) and the RGEMs research grant from VIT, Vellore.

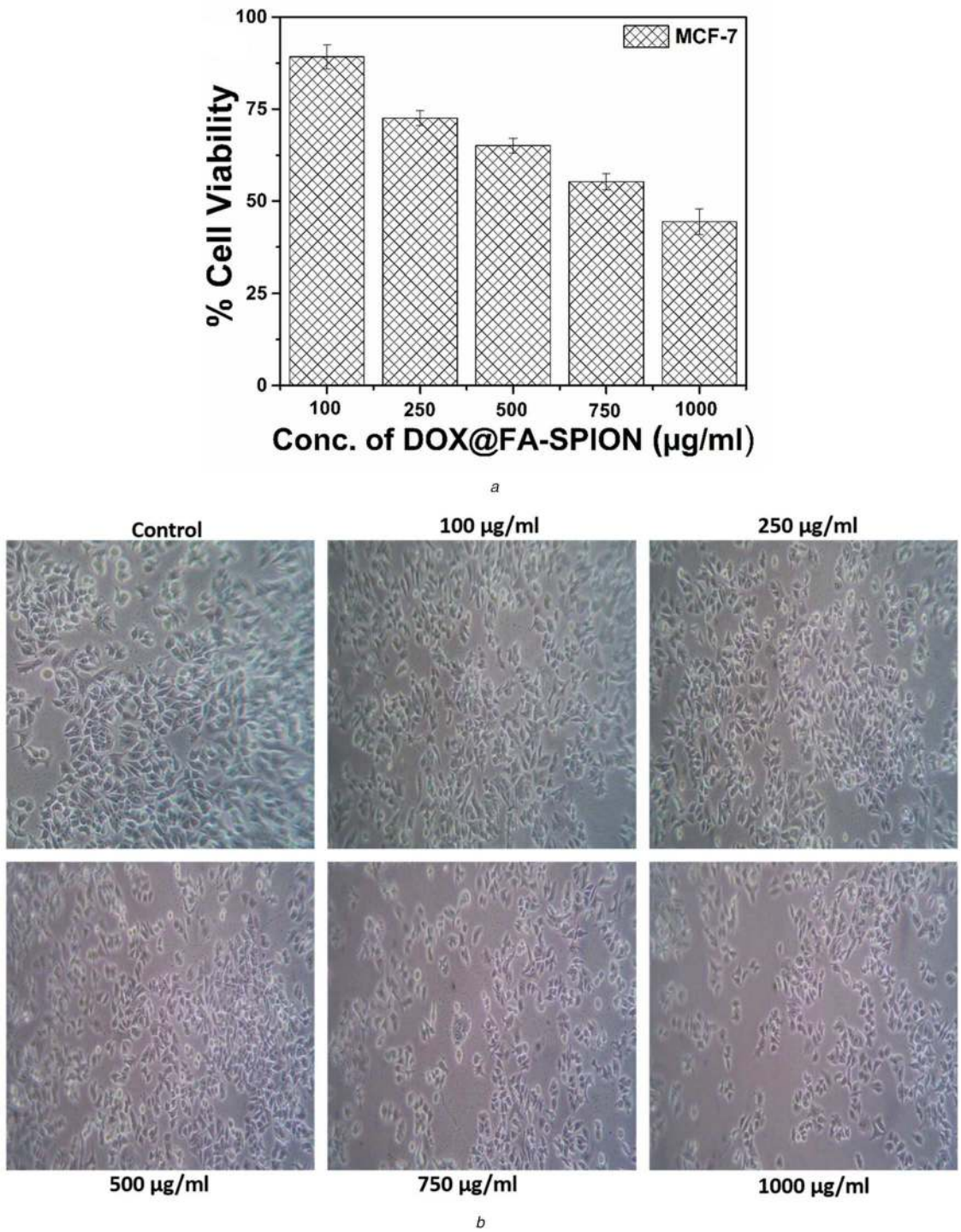

Fig. 6 *Viability after 24 h*

(a) Cytotoxicity assay,

(b) Optical images of DOX@FA-SPION with different concentration against MCF-7 breast cancer cells

6 References

[1] Khan, A., Arunima Rajan, S., Chandunika, R.K., *et al.*: 'Magneto-plasmonic stimulated breast cancer nanomedicine', in Thorat, N.D., Bauer, J. (Eds.): '*External field and radiation stimulated breast cancer nanotheranostics*' (IOP Publishing, UK, 2019, 1st edn.), pp. 5-1–5-27

[2] Mudshinge, S.R., Deore, A.B., Patil, S., *et al.*: 'Nanoparticles: emerging carriers for drug delivery', *Saudi Pharm. J.*, 2011, **19**, (3), pp. 129–141

[3] Irving, B.: 'Nanoparticle drug delivery systems', *Innov. Pharm. Technol.*, 2007, **24**, pp. 58–62

[4] Huang, Y., Mao, K., Zhang, B., *et al.*: 'Superparamagnetic iron oxide nanoparticles conjugated with folic acid for dual target-specific drug delivery and MRI in cancer theranostics', *Mater. Sci. Eng. C. Mater. Biol. Appl.*, 2017, **70**, (Pt 1), pp. 763–771

[5] Scialabba, C., Puleio, R., Peddis, D., *et al.*: 'Folate targeted coated spions as efficient tool for MRI', *Nano. Res.*, 2017, **10**, (9), pp. 3212–3227

[6] Carvalho, A., Martins, M.B.F., Corvo, M.L., *et al.*: 'Enhanced contrast efficiency in MRI by PEGylated magnetoliposomes loaded with PEGylated SPION: effect of spion coating and micro-environment', *Mater. Sci. Eng.: C*, 2014, **43**, pp. 521–526

[7] Lee, N., Yoo, D., Ling, D., *et al.*: 'Iron oxide based nanoparticles for multimodal imaging and magnetoresponsive therapy', *Chem. Rev.*, 2015, **115**, (19), pp. 10637–10689

[8] Xu, H.L., Mao, K.L., Huang, Y.P., *et al.*: 'Glioma-targeted superparamagnetic iron oxide nanoparticles as drug-carrying vehicles for theranostic effects', *Nanoscale*, 2016, **8**, (29), pp. 14222–14236

[9] Zhang, L., Rong, P., Chen, M., *et al.*: 'A novel single walled carbon nanotube (SWCNT) functionalization agent facilitating in-vivo combined chemo/thermo therapy', *Nanoscale*, 2015, **7**, (39), pp. 16204–16213

[10] Lee, S., Shieh, M.: 'Platinum (II) drug-loaded gold nanoshells for chemo-photothermal therapy in colorectal cancer', *ACS Appl. Mater. Interfaces*, 2020, **12**, (4), pp. 4254–4264

[11] Hervault, A., Thanh, N.T.K.: 'Magnetic nanoparticle - based therapeutic agents for thermo-chemotherapy treatment of cancer', *Nanoscale*, 2014, **6**, (20), pp. 11553–11573

[12] Chen, Y., Chen, P., Hu, S., *et al.*: 'NIR-triggered synergic photo-chemothermal therapy delivered by reduced graphene oxide/carbon/ mesoporous silica nanocookies', *Adv. Funct. Mater.*, 2014, **24**, (4), pp. 451–459

[13] Kumar, S., Daverey, A., Sahu, N.K., *et al.*: 'In vitro evaluation of PEGylated mesoporous $MgFe_2O_4$ magnetic nanoassemblies (MMNs) for chemo-thermal therapy', *J. Mater. Chem. B*, 2013, **1**, (30), pp. 3652–3660

[14] Rajan, S.A., Sahu, N.K.: 'Inductive calorimetric assesment of iron oxide nano-octahedrons for magnetic fluid hyperthermia', *Colloids Surf. A Physiochem. Eng. Asp.*, 2020, **603**, pp. 1–29

[15] Hayashi, K., Sato, Y., Sakamoto, W., *et al.*: 'Theranostic nanoparticles for MRI-guided thermochemotherapy: 'tight' clustering of magnetic nanoparticles boosts relaxivity and heat-generation power', *ACS Biomater. Sci. Eng.*, 2017, **3**, (1), pp. 95–105

[16] Sahu, N.K., Gupta, J., Bahadur, D.: 'PEGylated FePt-Fe3O4 composite nanoassemblies (CNAs): in vitro hyperthermia, drug delivery and generation of reactive oxygen species (ROS)', *Dalton Trans.*, 2015, **44**, (19), pp. 9103–9113

[17] Mahmoudi, M., Simchi, A., Milani, A.S., *et al.*: 'Cell toxicity of superparamagnetic iron oxide nanoparticles', *J. Colloid Interface Sci.*, 2009, **336**, (2), pp. 510–518

[18] Mahmoudi, M., Simchi, A., Imani, M.: 'Cytotoxicity of uncoated and polyvinyl alcohol coated superparamagnetic iron oxide nanoparticles', *J. Phys. Chem. C*, 2009, **113**, (22), pp. 9573–9580

[19] Viali, W., Nunes, E., Santos, C., *et al.*: 'PEGylation of SPIONs by polycondensation reactions: a new strategy to improve colloidal stability in biological media', *J. Nanopart. Res.*, 2013, **15**, pp. 1–14

[20] Balasubramaniam, S., Pothayee, N., Lin, Y., *et al.*: 'Poly(N-isopropylacrylamide)-coated superparamagnetic iron oxide nanoparticles: relaxometric and fluorescence behavior correlate to temperature-dependent aggregation', *Chem. Mater.*, 2011, **23**, (14), pp. 3348–3356

[21] Yar, Y., Khodadust, R., Akkoc, Y., *et al.*: 'Development of tailored SPION-PNIPAM nanoparticles by ATRP for dually responsive doxorubicin delivery and MR imaging', *J. Mater. Chem. B*, 2018, **6**, (2), pp. 289–300

[22] Liao, S., Liu, C., Bastakoti, B.P., *et al.*: 'Functionalized magnetic iron oxide/ alginate core-shell nanoparticles for targeting hyperthermia', *Int. J. Nanomedicine*, 2015, **10**, pp. 3315–3328

[23] Khalkhali, M., Sadighian, S., Rostamizadeh, K., *et al.*: 'Synthesis and characterization of dextran coated magnetite nanoparticles for diagnostics and therapy', *BioImpacts*, 2015, **5**, (3), pp. 141–150

[24] Luo, B., Xu, S., Luo, A., *et al.*: 'Mesoporous biocompatible and acid-degradable magnetic colloidal nanocrystal clusters with sustainable stability and high hydrophobic drug loading capacity', *ACS Nano*, 2011, **5**, (2), pp. 1428–1435

[25] Ziarani, G.M., Malmir, M., Lashgari, N., *et al.* 'The role of hollow magnetic nanoparticles in drug delivery', *RSC Adv.*, 2019, **9**, (43), pp. 25094–25106

[26] Gupta, J., Mohapatra, J., Bhargava, P., *et al.*: 'A pH - responsive folate conjugated magnetic nanoparticle for targeted chemo - thermal therapy and MRI diagnosis', *Dalton Trans.*, 2016, **45**, (6), pp. 2454–2461

[27] Byrne, J.D., Betancourt, T., Brannon-Peppas, L.: 'Active targeting schemes for nanoparticle systems in cancer therapeutics', *Adv. Drug Deliv. Rev.*, 2008, **60**, (15), pp. 1615–1626

[28] Sudimack, J., Lee, R.J.: 'Targeted drug delivery via the folate receptor', *Adv. Drug Delivery Rev.*, 2000, **41**, (2), pp. 147–162

[29] Turek, J.J., Leamon, C.P., Low, P.S.: 'Endocytosis of folate-protein conjugates: ultrastructural localization in KB cells', *J. Cell Sci.*, 1993, **106**, (Pt 1), pp. 423–430

[30] Angelopoulou, A., Kolokithas-Ntoukas, A., Fytas, C., *et al.*: 'Folic acid-functionalized, condensed magnetic nanoparticles for targeted delivery of doxorubicin to tumor cancer cells overexpressing the folate receptor', *ACS Omega*, 2019, **4**, (26), pp. 22214–22227

[31] Yang, C., Chen, J., Wei, K., *et al.*: 'Release of doxorubicin by a folate-grafted, chitosan-coated magnetic nanoparticle', *Nanomaterials*, 2017, **7**, (4), pp. 1–12

[32] Parker, N., Turk, M.J., Westrick, E., *et al.*: 'Folate receptor expression in carcinomas and normal tissues determined by a quantitative radioligand binding assay', *Anal. Biochem.*, 2005, **338**, (2), pp. 284–293

[33] Dixit, V., Van den Bossche, J., Sherman, D.M., *et al.*: 'Synthesis and grafting of thioctic acid − PEG − folate conjugates onto au nanoparticles for selective targeting of folate receptor-positive tumor cells', *Bioconjugate Chem.*, 2006, **17**, (3), pp. 603–609

[34] Elnakat, H., Ratnam, M.: 'Distribution, functionality and gene regulation of folate receptor isoforms: implications in targeted therapy', *Adv. Drug Delivery Rev.*, 2004, **56**, (8), pp. 1067–1084

[35] Sahoo, B., Devi, K.S.P., Banerjee, R., *et al.*: 'Thermal and pH responsive polymer-tethered multifunctional magnetic nanoparticles for targeted delivery of anticancer drug', *ACS Appl. Mater. Interfaces*, 2013, **5**, (9), pp. 3884–3893

[36] Rani, B., Punniyakoti, S., Sahu, N.K.: 'Polyol asserted hydrothermal synthesis of SnO_2 nanoparticles for the fast adsorption and photocatalytic degradation of methylene blue cationic dye', *New J. Chem.*, 2018, **42**, (2), pp. 943–954

[37] Tenório-Neto, E.T., Jamshaid, T., Eissa, M., *et al.*: 'TGA and magnetization measurements for determination of composition and polymer conversion of magnetic hybrid particles', *Polym. Adv. Technol.*, 2015, **26**, (10), pp. 1199–1208

[38] Zhang, C., Zhao, L., Dong, Y., *et al.* 'Folate-mediated poly(3-hydroxybutyrate-co-3-hydroxyoctanoate) nanoparticles for targeting drug delivery', *Eur. J. Pharm. Biopharm.*, 2010, **76**, (1), pp. 10–16

[39] Ahangaran, F., Hassanzadeh, A., Nouri, S.: 'Surface modification of Fe_3O_4@SiO_2 microsphere by silane coupling agent', *Int. Nano Lett.*, 2013, **3**, pp. 1–5

[40] Bartczak, D., Kanaras, A.G., 'Preparation of peptide-functionalized gold nanoparticles using one pot EDC/sulfo-NHS coupling', *Langmuir*, 2011, **27**, (16), pp. 10119–10123

[41] Faraji, A.H., Wipf, P.: 'Nanoparticles in cellular drug delivery', *Bioorg. Med. Chem.*, 2009, **17**, (8), pp. 2950–2962

[42] Biswas, A.K., Islam, M.R., Choudhury, Z.S., *et al.*: 'Nanotechnology based approaches in cancer therapeutics', *Adv. Nat. Sci.: Nanosci. Nanotechnol.*, 2014, **5**, (4), pp. 1–11

[43] Chithrani, B.D., Ghazani, A.A., Chan, W.C.W.: 'Determining the size and shape dependence of gold nanoparticle uptake into mammalian cells', *Nano Lett.*, 2006, **6**, (4), pp. 662–668

[44] Zhang, K., Fang, H., Chen, Z., *et al.*: 'Shape effects of nanoparticles conjugated with cell-penetrating peptides (HIV tat PTD) on CHO cell uptake', *Bioconjugate Chem.*, 2008, **19**, (9), pp. 1880–1887

[45] Neha, R., Jaiswal, A., Bellare, J., *et al.*: 'Synthesis of surface grafted mesoporous magnetic nanoparticles for cancer therapy', *J. Nanosci. Nanotechnol.*, 2017, **17**, (8), pp. 5181–5188

[46] Thommes, M., Kaneko, K., Neimark, A.V., *et al.*: 'Physisorption of gases, with special reference to the evaluation of surface area and pore size distribution (iupac technical report)', *Pure Appl. Chem.*, 2015, **87**, (10), pp. 1051–1069

[47] Hanaor, D., Michelazzi, M., Leonelli, C., *et al.*: 'The effects of carboxylic acids on the aqueous dispersion and electrophoretic deposition of ZrO_2', *J. Eur. Ceram. Soc.*, 2012, **32**, (1), pp. 235–244

[48] Pradhan, L., Srivastava, R., Bahadur, D., 'Ph- and thermosensitive thin lipid layer coated mesoporous magnetic nanoassemblies as a dual drug delivery system towards thermochemotherapy of cancer', *Acta Biomater.*, 2014, **10**, (7), pp. 2976–2987

[49] Chandra, S., Mehta, S., Nigam, S., *et al.*: 'Dendritic magnetite nanocarriers for drug delivery applications', *New J. Chem.*, 2010, **34**, (4), pp. 648–655

[50] Prabha, G., Raj, V.: 'Formation and characterization of Beta-cyclodextrin (Beta-CD) - polyethyleneglycol (PEG) - polyethyleneimine (PEI) coated Fe_3O_4 nanoparticles for loading and releasing 5-fluorouracil drug', *Biomed. Pharmacother.*, 2016, **80**, pp. 173–182

[51] Rezaian, M., Maleki, R., Dahri Dahroud, M., *et al.*: 'Ph-sensitive Co-adsorption/release of doxorubicin and paclitaxel by carbon nanotube, fullerene, and graphene oxide in combination with N-isopropylacrylamide: a molecular dynamics study', *Biomolecules*, 2018, **8**, (4), pp. 1–21

[52] Wu, H., Yin, J., Wamer, W.G., *et al.*: 'Reactive oxygen species-related activities of nano-iron metal and nano-iron oxides', *J. Food Drug Anal.*, 2014, **22**, (1), pp. 86–94

[53] Xu, C., Yuan, Z., Kohler, N., *et al.*: 'Fept nanoparticles as an Fe reservoir for controlled Fe release and tumor inhibition', *J. Am. Chem. Soc.*, 2009, **131**, (42), pp. 15346–15351

[54] Valko, M., Rhodes, C.J., Moncol, J., *et al.*: 'Free radicals, metals and antioxidants in oxidative stress-induced cancer', *Chem.-Biol. Interact.*, 2006, **160**, (1), pp. 1–40

[55] Pilco-Ferreto, N., Calaf, G.M.: 'Influence of doxorubicin on apoptosis and oxidative stress in breast cancer cell lines', *Int. J. Oncol.*, 2016, **49**, (2), pp. 753–762